

# Spectral signatures of modulated $d$ -wave superconducting phases

Shirit Baruch and Dror Orgad

*Racah Institute of Physics, The Hebrew University, Jerusalem 91904, Israel*

(Dated: November 2, 2018)

We calculate within a mean-field theory the spectral signatures of various striped  $d$ -wave superconducting phases. We consider both in-phase and anti-phase modulations of the superconducting order across a stripe boundary, and the effects of coexisting inhomogeneous orders, including spin stripes, charge stripes, and modulated  $d$ -density-wave. We find that the anti-phase modulated  $d$ -wave superconductor exhibits zero-energy spectral weight, primarily along extended arcs in momentum space. Concomitantly, a Fermi surface appears and typically includes both open segments and closed pockets. When weak homogeneous superconductivity is also present the Fermi surface collapses onto nodal points. Among them are the nodal points of the homogeneous  $d$ -wave superconductor, but others typically exist at positions which depend on the details of the modulation and the band structure. Upon increasing the amplitude of the constant component these additional points move towards the edges of the reduced Brillouin zone where they eventually disappear. The above signatures are also manifested in the density of states of the clean, and the disordered system. While the presence of coexisting orders changes some details of the spectral function, we find that the evolution of the Fermi-surface and the distribution of the low-energy spectral weight are largely unaffected by them.

PACS numbers: 74.81.-g, 74.25.Jb, 74.20.-z, 74.72.-h

## I. INTRODUCTION

Over the last decade it has become increasingly clear that the cuprate high-temperature superconductors exhibit inhomogeneous electronic structures both in their "normal" and superconducting states<sup>1</sup>. In particular, several scanning tunneling spectroscopy experiments have produced evidence for real-space inhomogeneity of the superconducting gap without apparent spatial ordering<sup>2-7</sup>, while others have demonstrated periodic modulations of the local density of states (LDOS)<sup>8-17</sup>. Even if much of the modulated signal can be attributed to interference patterns resulting from scattering of quasiparticles off impurities<sup>9,10,19</sup>, at least part of it is likely associated with a spatially periodic structure of the superconducting order and possibly of other coexisting electronic orders<sup>11-18</sup>.

In this paper we study, within mean field theory, various realizations of modulated  $d$ -wave superconducting (DSC) phases. We focus on stripe phases in which the lattice-translational invariance is broken in one direction, and calculate their spectral signatures in the clean limit and in the presence of disorder. The quasiparticle density of states of clean translational-symmetry breaking states has been calculated by Podolsky *et al.* in Ref. 20. There, the effects of a small modulated order parameter added to a large-amplitude  $d$ -wave superconductor, were investigated. Here we extend this treatment to strong modulations, consider also the distribution of spectral weight in momentum space, and study additional scenarios which were not treated in Ref. 20. In particular, we analyze the case of an anti-phase modulated superconductivity, where the  $d$ -wave order parameter suffers a  $\pi$ -phase shift across each stripe boundary. Such a state has been proposed recently<sup>21,22</sup> as the source for

the apparent decoupling between the Cu-O planes in 1/8 doped  $\text{La}_{2-x}\text{Ba}_x\text{CuO}_4$ <sup>23</sup>. Similar structures were also found in a mean-field study of the DSC resonating valence bond phase of the  $t-J$  model<sup>24</sup>. Finally, we supplement the extensive literature on the Fourier-transformed local density of states (FT-LDOS) of disordered superconducting phases, with and without coexisting inhomogeneous orders<sup>25-37</sup>, by calculating the FT-LDOS of a system with anti-phase modulated superconductivity.

We demonstrate that in sharp contrast to its homogeneous and in-phase modulated counterparts, the anti-phase modulated  $d$ -wave superconductor exhibits a Fermi surface which includes extended parts of the non-interacting Fermi-surface, as well as closed pockets. The corresponding zero-energy spectral weight appears predominantly over arcs in momentum space, whose extent shrinks with increasing amplitude of the order parameter. We find that this general behavior is robust with respect to changes in the details of the band-structure and in the functional form of the modulations. Furthermore, the general evolution of the Fermi-surface and the distribution of low-energy spectral weight is largely unaffected by the introduction of additional coexisting orders. The situation changes significantly when a homogeneous superconducting component is also present in the system. Under such conditions the Fermi-surface collapses onto nodal points, which include those of the homogeneous  $d$ -wave superconductor, and generically, additional points at positions which depend on details of the modulation and band-structure. Upon increasing the constant order parameter the extra nodal points move towards the edges of the reduced Brillouin zone (BZ), where they eventually disappear. The presence of the Fermi-surface is also reflected in the low-energy density of states of the anti-phase modulated DSC state, and in the momentum-space structure of the FT-LDOS of this system when impurity

scattering is included in the analysis.

## II. THE MODELS

Our starting point is a tight binding model of electrons hopping on a square lattice. In the following we consider two non-interacting band structures, corresponding to  $\text{Bi}_2\text{Sr}_2\text{CaCu}_2\text{O}_{8+\delta}$  and  $\text{La}_{2-x}\text{Ba}_x\text{CuO}_4$ . While most of the scanning tunneling experiments have been carried out on the first, owing to the good quality of surfaces which can be obtained in this system, the latter is probably the most promising compound for the observation of the signatures we discuss in the following, especially in the context of anti-phase modulated superconductivity. Consequently, most of our results will be presented for this material. To model  $\text{Bi}_2\text{Sr}_2\text{CaCu}_2\text{O}_{8+\delta}$  we use the tight-binding Hamiltonian provided by Norman *et. al.*<sup>38</sup>, for the system near optimal doping. The 1/8 hole-doped  $\text{La}_{2-x}\text{Ba}_x\text{CuO}_4$  is described by the free dispersion<sup>39</sup>  $\xi(\mathbf{k}) = -(t_1/2)[\cos(k_x) + \cos(k_y)] - t_2 \cos(k_x) \cos(k_y) - \mu$ , where  $t_1 = 1.72$  eV,  $t_2 = -0.15t_1$  and  $\mu$  is the chemical potential which we adjust in order to maintain the required level of hole-doping.

In this work we study, using a mean-field Hamiltonian, the spectral signatures of a spatially modulated  $d$ -wave superconductor. We also consider within the same approximation, the effects of other inhomogeneous coexisting orders on such properties. Motivated by the experimental evidence for the existence of "stripes" in the high-temperature superconductors<sup>1</sup>, we analyze the case where the discrete translation symmetry of the underlying lattice is broken by the periodic orders in the  $x$  direction. Since often the observed charge and spin modulation periods are 4 and 8 lattice constants, respectively, we assume a unit cell of either lengths for the modulated orders. In the following we describe the real-space structure of the various configurations which are studied in the paper.

### A. The superconducting order

We consider two configurations for the DSC order. In the first its magnitude is sinusoidally modulated across each site-centered stripe, but its phase is constant over the sample. This "in-phase" configuration is described by the mean-field Hamiltonian

$$H_{0-dSC} = \sum_{x,y} \left\{ \frac{\Delta}{4} |\cos[q_x(x+1/2)]| \times \left[ c_{x,y\uparrow}^\dagger c_{x+1,y\downarrow}^\dagger - c_{x,y\downarrow}^\dagger c_{x+1,y\uparrow}^\dagger \right] - \frac{\Delta}{4} |\cos(q_x x)| \times \left[ c_{x,y\uparrow}^\dagger c_{x,y+1\downarrow}^\dagger - c_{x,y\downarrow}^\dagger c_{x,y+1\uparrow}^\dagger \right] + \text{H.c.} \right\}, \quad (1)$$

where  $x$  and  $y$  are measured in units of the lattice constant which we take from now on to be 1. Here, and throughout the paper  $q_x = \pi/4$ . Note, that since the order parameter does not change its sign across the stripe boundary the resulting configuration has a 4-site unit cell, as presented in Fig. 1. On a microscopic level it may reflect a variation in the pairing amplitude as a result of a corresponding modulation of the hole density in the stripe phase, as discussed below.

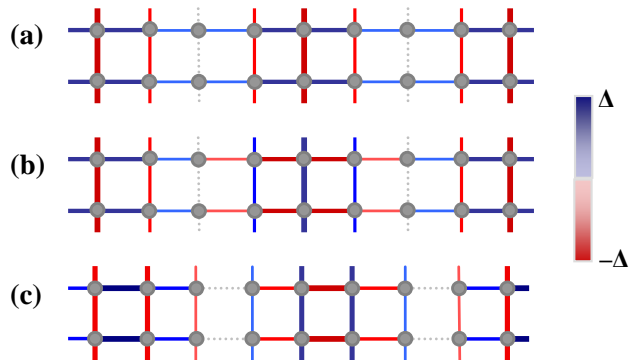


FIG. 1: The DSC configurations considered in this work: a) site-centered in-phase modulated, and b) site-centered anti-phase modulated. c) bond-centered anti-phase modulated. The magnitude of the order parameter is depicted by the width of the lines, while its sign is given by the colors of the bonds.

The second, "anti-phase", configuration is similar to the first, except that the phase of the order parameter changes by  $\pi$  across a stripe boundary. It has been suggested in Ref. 21, that despite being unconventional, such a negative Josephson coupling between stripes may occur in 1/8 doped  $\text{La}_{2-x}\text{Ba}_x\text{CuO}_4$ , with significant consequences for the transport through this system. We consider the site-centered version of the configuration, see Fig. 1, and analyze the Hamiltonian

$$H_{\pi-dSC} = \sum_{x,y} \left\{ \frac{\Delta}{4} \cos[q_x(x+1/2)] \times \left[ c_{x,y\uparrow}^\dagger c_{x+1,y\downarrow}^\dagger - c_{x,y\downarrow}^\dagger c_{x+1,y\uparrow}^\dagger \right] - \frac{\Delta}{4} \cos(q_x x) \times \left[ c_{x,y\uparrow}^\dagger c_{x,y+1\downarrow}^\dagger - c_{x,y\downarrow}^\dagger c_{x,y+1\uparrow}^\dagger \right] + \text{H.c.} \right\}. \quad (2)$$

The anti-phase nature of the configuration results in an 8-site unit cell.

We have also considered the bond-centered analogs of the above site-centered configurations. Fig. 1 depicts, for example, the bond-centered anti-phase modulated DSC. We have found, however, that the results are hardly affected by this detail, and therefore in the following we report them for the site-centered orders.

## B. Coexisting electronic orders

Various electronic orders have been proposed to exist in the cuprate high-temperature superconductors, especially in the underdoped regime. In this paper we consider the case where the modulated superconducting order is accompanied by one or more of the following: charge stripes, anti-phase spin stripes and an anti-phase modulated  $d$ -density wave (DDW).

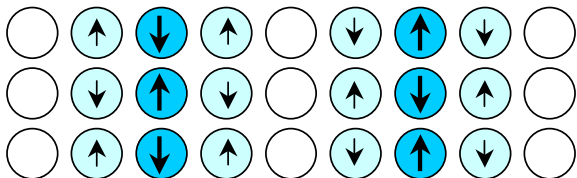


FIG. 2: A sketch of the magnetic and charge distribution in the stripe model. The arrows represent the amplitude and sign of the spin density, and the shading of the circles represents the charge density (the darker the circle is, the higher the charge density).

For the charge stripe phase we assume a site-centered, period-4 sinusoidal charge density  $\langle n_{x,y\uparrow} + n_{x,y\downarrow} \rangle = \phi_{CDW} |\sin(q_x x)|$ . When spin stripe order is also present the boundaries of the charge unit-cells serve as anti-phase domain walls for an antiferromagnetic (AF) spin order of the form  $\langle n_{x,y\uparrow} - n_{x,y\downarrow} \rangle = \phi_{AF} (-1)^{x+y} \sin(q_x x)$ . The combined charge-spin stripe configuration is depicted in Fig. 2, and the corresponding Hamiltonian is described in appendix A.

The uniform DDW state was proposed as a model for the pseudogap state in the underdoped cuprates<sup>40</sup>. It describes a condensation of electron-hole pairs with non-zero angular momentum into a phase with staggered current loops. In the following we consider the anti-phase, period-8, modulated version of this state as displayed in Fig. 3. Note that current conservation has been incorporated into the model. For a detailed expressions of the order parameter and the mean field Hamiltonian see appendix A.

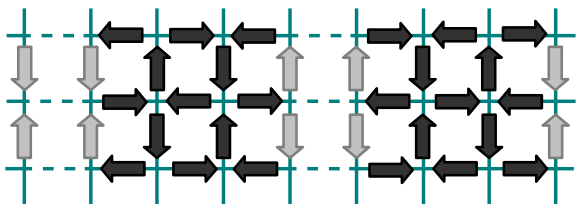


FIG. 3: A schematic representation of the modulated DDW order parameter. The arrows represent the currents in the system. Gray arrows carry half the current of the black ones.

## III. RESULTS

### A. The Fermi-surface and the distribution of low-energy spectral weight

It is well known that the Fermi-surface of a homogeneous  $d$ -wave superconductor consists of four nodal points. A very different behavior emerges in the case of an anti-phase modulated DSC, as shown by Fig. 4. The figure exhibits the evolution of the Fermi-surface of  $\text{La}_{2-x}\text{Ba}_x\text{CuO}_4$  with increasing strength,  $\Delta$ , of the anti-phase modulated DSC, where the chemical potential is adjusted to maintain a  $1/8$  hole-doping level for each set of parameters. One can clearly see that the model supports an extended Fermi-surface. As the amplitude  $\Delta$  increases, segments of the non-interacting Fermi-surface near  $(0, \pi)$  and symmetry related regions, become progressively gapped. At the same time the Fermi-surface develops closed pockets which shrink with increasing  $\Delta$  and eventually disappear completely. The process proceeds until a single pocket remains when  $\Delta$  is of the order of the band-width. It then continues to shrink upon further increase of the DSC order. This behavior is generic as can be seen in Fig. 5, where similar results are presented for  $\text{Bi}_2\text{Sr}_2\text{CaCu}_2\text{O}_{8+\delta}$ . The rate at which the Fermi-surface evolves, depends, however, on the band-structure. The flatter sections in the anti-nodal regions of  $\text{Bi}_2\text{Sr}_2\text{CaCu}_2\text{O}_{8+\delta}$  tend to develop a gap more quickly than the rest of the Fermi-surface.

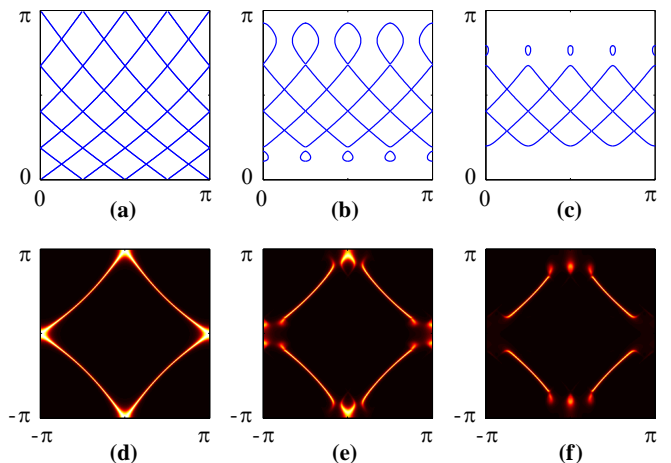


FIG. 4: The Fermi Surface (a)-(c), and the low-energy spectral weight (d)-(f) of a model corresponding to  $1/8$  hole-doped  $\text{La}_{2-x}\text{Ba}_x\text{CuO}_4$  in the presence of an anti-phase modulated DSC. The Fermi surface is plotted in the first quadrant of the Brillouin zone. The spectral weight is integrated within a 20 meV Lorentzian window centered at zero energy. The amplitude of the modulated DSC is  $\Delta = 0$  in (a,d),  $\Delta = 0.075t_1$  in (b,e) and  $\Delta = 0.15t_1$  in (c,f).

We believe that the origin of the Fermi-surface can be traced to the formation of zero-energy Andreev bound states on the anti-phase domain walls of the DSC or-

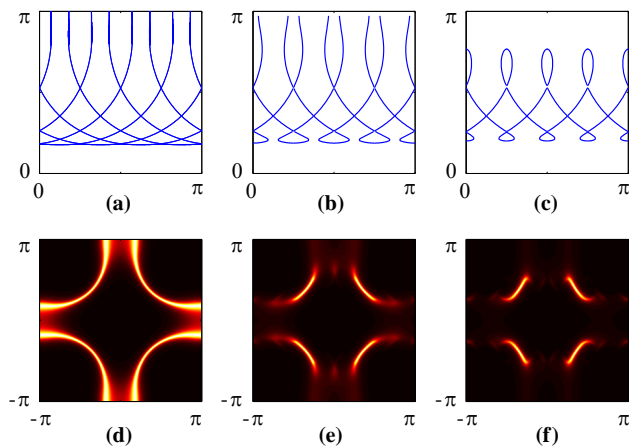


FIG. 5: The Fermi Surface and the low-energy spectral weight in a model of 17% hole-doped  $\text{Bi}_2\text{Sr}_2\text{CaCu}_2\text{O}_{8+\delta}$  with anti-phase modulated DSC. The spectral weight was integrated in a similar manner to Fig. 4. The results are given for  $\Delta = 0$  in (a,d),  $\Delta = 0.075t$  in (b,e), and  $\Delta = 0.15t$  in (c,f) ( $|t| \simeq 0.6$  eV, see Ref. 38.)

der. A single junction between two phase-biased  $d$ -wave superconductors has been studied by Tanaka and Kashiwaya<sup>41</sup>. They have calculated the quasiparticle LDOS at the interface between the superconductors and demonstrated that for a  $\pi$ -phase shift the LDOS displays a pronounced zero-bias peak, associated with zero-energy Andreev bound states. The latter move to higher energies when the phase difference is tuned away from  $\pi$ , and correspondingly the LDOS exhibits a pseudo-gap behavior at low biases. In our model we consider a chain of such junctions and therefore must take into account the multiple scattering processes between them. We have not carried out a detailed analytical analysis of this problem. Nevertheless, the numerical real-space structure of the zero-energy wavefunctions reveal that the states residing near the end-points of the open Fermi-surface segments are indeed localized on the domain walls. On the other hand, the zero-energy states on the Fermi-pockets and away from these end points are approximately evenly distributed over the system.

Angle resolved photoemission spectroscopy (ARPES) is arguably the most suitable probe for detecting the extended Fermi-surface. More generally, ARPES measures the spectral function  $A(\mathbf{k}, \omega)$  of the system. In Figs. 4, 5 we plot the distribution of low-energy spectral weight of an anti-phase modulated  $d$ -wave superconductor, namely the frequency integrated  $A(\mathbf{k}, \omega)$  within a 20 meV Lorentzian window centered at zero energy. As shown in the figures, the spectral weight lies predominantly along arcs in momentum space. As we increase the superconducting order the arcs shrink towards the BZ diagonals. For the sinusoidal modulation studied here the distribution of spectral weight along the arcs is continuous. However, for a square-wave modulation, gaps open on the arcs at the boundaries of the reduced BZ at  $k_x = \pm\pi/8$  and

at points which are related to them by the modulation wavevector.

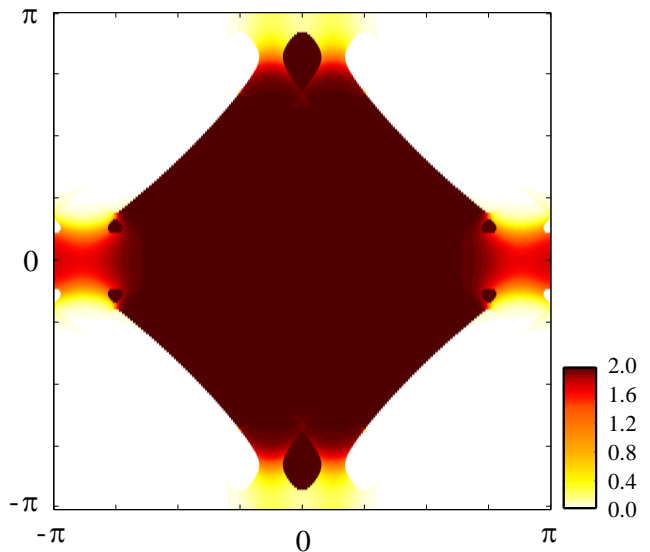


FIG. 6: The momentum occupation function  $n(\mathbf{k})$  of a model of 1/8 hole-doped  $\text{La}_{2-x}\text{Ba}_x\text{CuO}_4$  with an anti-phase modulated DSC of strength  $\Delta = 0.075t_1$ .

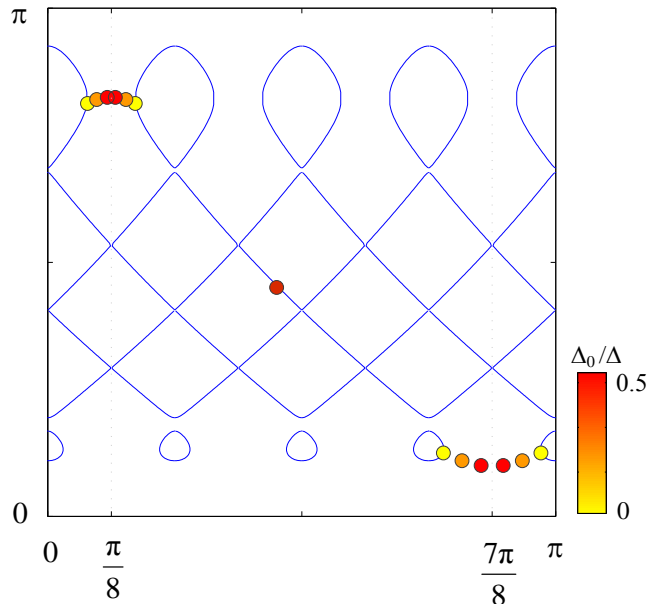


FIG. 7: The evolution of the nodal points in a model of 1/8 hole-doped  $\text{La}_{2-x}\text{Ba}_x\text{CuO}_4$  with anti-phase modulated DSC of strength  $\Delta = 0.075t_1$ , as function of the amplitude,  $\Delta_0$ , of an additional homogeneous DSC component. The curve depicts the Fermi-surface for the case  $\Delta_0 = 0$ .

ARPES can also provide a measurement of the momentum occupation function  $n(\mathbf{k}) = \int_{-\infty}^0 (d\omega/2\pi) A(\mathbf{k}, \omega)$ . It is this function which depicts most directly the presence of the closed segments, or "pockets", in the Fermi-surface. Fig. 6 displays  $n(\mathbf{k})$  for the anti-phase mod-

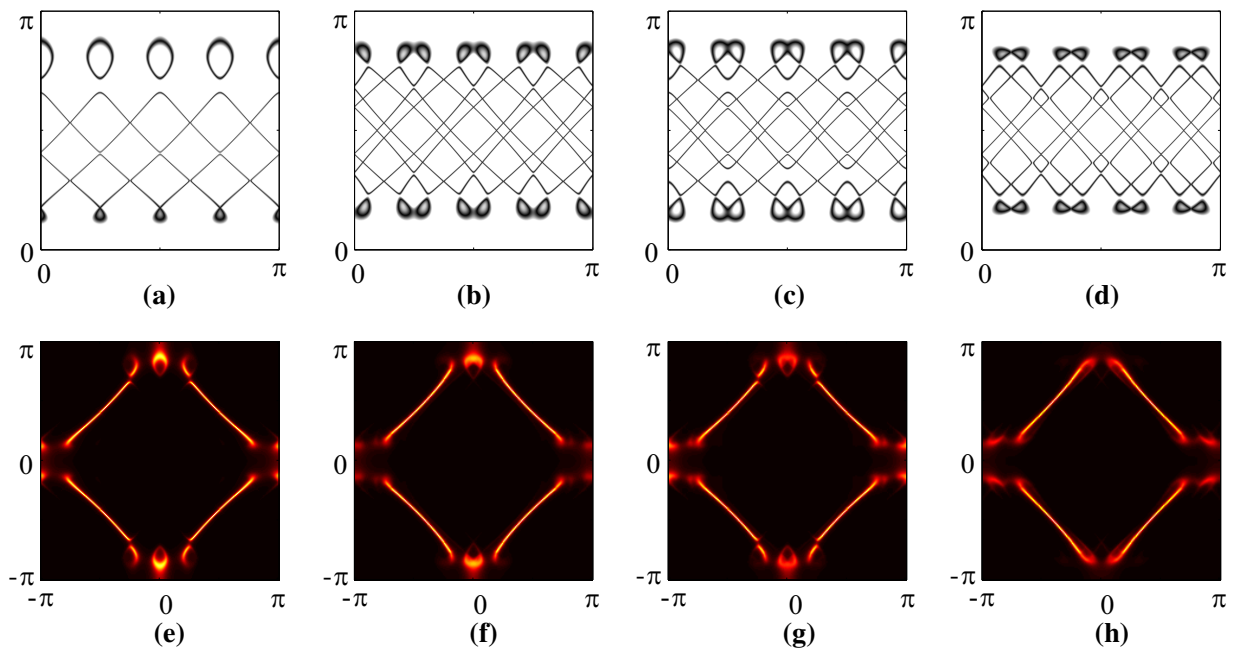


FIG. 8: Fermi surfaces (a)-(d) and low-energy spectral weight distributions (e)-(h) of a model corresponding to 1/8 hole-doped  $\text{La}_{2-x}\text{Ba}_x\text{CuO}_4$  with anti-phase modulated DSC and additional orders. The amplitude of the DSC order parameter is  $\Delta = 0.1t_1$ , and the additional orders are: in (a,e) CDW with  $\phi_{CDW} = 0.075t_1$ , (b,f) spin-stripe order with  $\phi_{AF} = 0.075t_1$ , (c,g) charge and spin stripe order with  $\phi_{AF} = \phi_{CDW} = 0.075t_1$ , (d,h) modulated DDW with  $\phi_{DDW} = 0.0125t_1$ . Note that the reduced BZ is halved in the presence of spin stripes or a modulated DDW, thus complicating a straightforward comparison between the different Fermi surfaces.

ulated DSC in  $\text{La}_{2-x}\text{Ba}_x\text{CuO}_4$ . While Fermi-surface pockets in the normal state can always be classified as electron-like or hole-like, this is no longer true for the superconductor whose quasiparticles are linear combinations of both electrons and holes. However, as can be seen from Fig. 6, the pockets at  $k_x \simeq 0$  and  $k_x \simeq \pm 3\pi/4$  are close to being electron-like, while the pockets at  $k_x \simeq \pm\pi$  are of the hole-like type. Recently, much interest has been generated by the observation of Shubnikov-de Haas and de Haas-van Alphen oscillations in underdoped  $\text{YBa}_2\text{Cu}_3\text{O}_{7-\delta}$  in strong magnetic fields which suppress superconductivity<sup>42,43</sup>. The experimental results suggest that the Fermi-surface contains coherent electron-like pockets. Theoretical studies of non-superconducting spin-charge modulated phases have found evidence for electron<sup>45</sup> and hole<sup>44</sup> pockets. Although unlikely to be relevant to the understanding of the aforementioned experiments, it would be interesting to investigate the impact of the pockets which we find in the anti-phase model, on the transport and magnetic properties of the system. We, however, did not pursue this direction.

When a constant DSC component, of arbitrary small magnitude, is added to the anti-phase modulated system the Fermi-surface changes dramatically and collapses onto nodal points. Among them we always find the nodal points of the uniform  $d$ -wave superconductor along the diagonals of the BZ. However, as demonstrated by Fig. 7, additional nodal points typically appear for not too large magnitude,  $\Delta_0$ , of the constant component. For

the parameters used by us their spectral weight is about a half of the weight of the points along the diagonals. When  $\Delta_0$  is increased, the additional points move from the tips of the pockets, where they originate, towards the edge of the reduced BZ where they disappear, while the points along the diagonals stay put. The number and positions of the nodal points vary as function of the strength of the modulated order and of the band-structure, but the general behavior remains the same. In the case of an in-phase modulated DSC we always find a Fermi-surface which consists of the four nodal points of the uniform superconductor. This is not surprising since the in-phase modulated order can be represented approximately as an equal strength combination of anti-phase and constant components, for which, as seen in Fig. 7, the extra nodal points have long vanished. It is worth mentioning that while the change in the topology of the Fermi-surface takes place even for an infinitesimal  $\Delta_0$ , the original Fermi-surface of the anti-phase modulated system is only gapped by an amount of order  $\Delta_0$ . Therefore, the low-energy spectral weight distribution of a system with weak additional homogeneous DSC is close to the one presented in Figs. 4, 5.

We have also studied the Fermi-surface and the low-energy spectral weight in the presence of additional electronic orders, as described in section II. At large, we have found that the coexisting orders do not change the general features outlined above. The Fermi-surface of the in-phase modulated system is still comprised of the

conventional  $d$ -wave nodal points. The introduction of the orders into the anti-phase modulated superconductor does have some effect on the Fermi-surface and the spectral weight distribution, as seen in Fig. 8 (Note that the reduced BZ is halved in the presence of spin stripes or a modulated DDW.) Most notably, we observe that the CDW order induce gaps on the Fermi-surface at multiples of the ordering wavevector. Although the shape of the Fermi-surface is somewhat different, its extent is largely unaffected by the additional orders. This is also true for the general evolution of the Fermi-surface with increasing  $\Delta$  and with the addition of a uniform DSC component.

### B. The density of states

The low-energy signatures discussed above are also manifested in the LDOS, which can be measured using scanning tunneling spectroscopy. Fig. 9 presents the density of states of the modulated superconducting states after averaging over the position in the sample. The energy dependence of the DOS in the case of the in-phase modulated DSC is close to that of a uniform  $d$ -wave superconductor whose amplitude is given by the zero-wavevector component of the modulated order. In particular, the DOS vanishes at zero-bias (In order to simulate the finite energy resolution of the experiments we have introduced

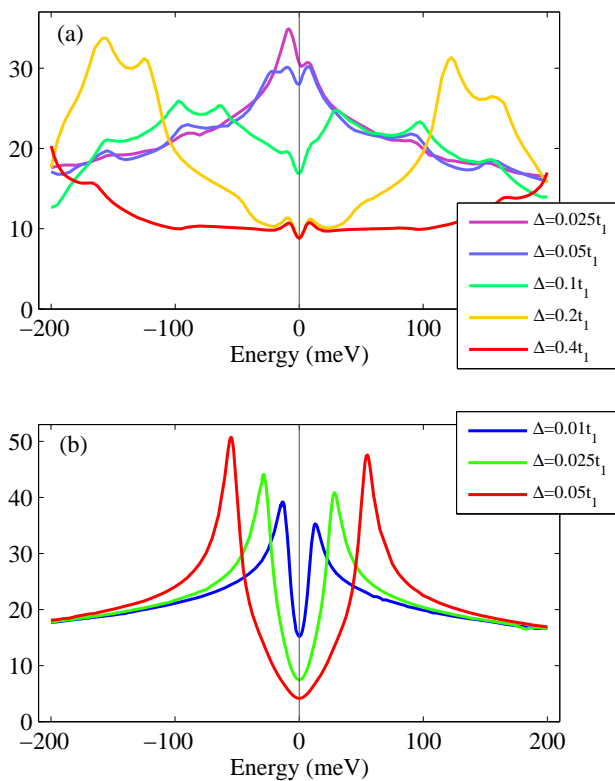


FIG. 9: Averaged density of states in a model of LBCO with (a) anti-phase modulated DSC and (b) in-phase modulated DSC, for various magnitudes of the superconducting order.

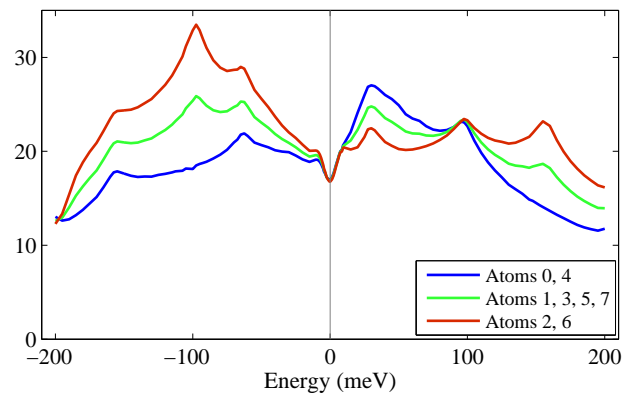


FIG. 10: LDOS in a model of  $\text{La}_{2-x}\text{Ba}_x\text{CuO}_4$  with an anti-phase modulated DSC of strength  $\Delta = 0.1t_1$ . Atom 0 is located on the symmetry axis of the stripe - the left most site in Fig. 1.

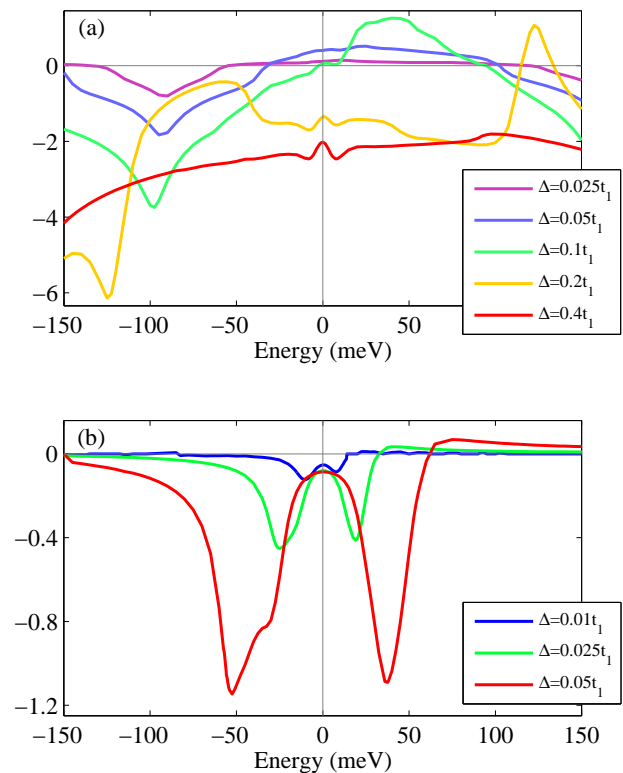


FIG. 11:  $\rho(\pi/2, 0)$  in a model of LBCO with (a) anti-phase modulated DSC and (b) in-phase modulated DSC, for various magnitudes of the superconducting order.

a 5 meV Lorentzian broadening into our numerical calculation. This is the reason for the apparent zero-energy DOS in the figure.) In contrast, the zero-energy DOS of the anti-phase modulated system remains finite. We find that the low-energy behavior of the DOS depends on the band-structure. For  $\text{La}_{2-x}\text{Ba}_x\text{CuO}_4$  the DOS contains a small dip at zero bias whose width does not scale with the strength of the modulated superconducting or-

der, see Fig. 9. In  $\text{Bi}_2\text{Sr}_2\text{CaCu}_2\text{O}_{8+\delta}$  on the other hand (not shown here), there is a more pronounced dip which does scale with  $\Delta$ . In both cases the low-energy DOS decreases when  $\Delta$  is increased, in agreement with the reduction in the extent of the Fermi-surface, as described above.

Although the unit-cell in the anti-phase superconducting system is composed of 8 sites, the real space periodicity of the LDOS is halved, as shown in Fig. 10. This is a result of the symmetries of the model. Translating the system by 4 lattice constants is equivalent to the change  $\Delta \rightarrow -\Delta$ , which does not affect the LDOS, as long as the average pairing potential is zero. An additional constant DSC component breaks this symmetry, opens a  $d$ -wave gap in the LDOS, and reverts its period to 8 sites. Consequently, the first non-vanishing Fourier component of the LDOS,  $(\rho_q(\omega))$ , in both the in-phase and the pure anti-phase modulated models is at  $\mathbf{q} = (\pi/2, 0)$ . Its energy dependence is shown in Fig. 11. While for the in-phase model it exhibits a symmetric structure around zero bias within the low-voltage regime, such symmetry is absent in the anti-phase case.

The addition of electronic orders to the superconducting system does not change the main features described above. Zero-bias spectral weight is still observed in the anti-phase DSC model and is absent in the in-phase system. The periodicity of the LDOS is also unaffected by the CDW and the DDW orders, while the spin-stripe order introduces new Fourier components at multiples of  $\mathbf{q} = (\pi/4, \pi)$ .

### C. FT-LDOS

In recent years, scanning tunneling spectroscopy measurements of the FT-LDOS have become a much-used tool in the quest for identifying unconventional electronic orders in the cuprates<sup>25</sup>. We have calculated the effects of quasiparticle scattering off a single impurity on the FT-LDOS in a system with modulated superconductivity. To this end we have implemented the T-matrix approximation, as described in appendix B.

Since most of the spectral changes in the modulated system occur at low energies we choose here to concentrate on the zero-energy FT-LDOS, and present, in Fig. 12, its distribution for an anti-phase modulated DSC system with, and without, an additional homogeneous DSC component. As can be seen, the Fourier transformed spectra is highly detailed. However, this fine structure is unlikely to be accessible experimentally as it is of very small weight compared to the prominent peaks which dominate the distribution. Consequently, we concentrate on the latter.

In both cases studied by us the strongest peaks appear at multiples of the modulation wavevector  $\mathbf{q} = (\pi/4, 0)$ . [Note that disorder eliminates the symmetry which produces the period-4 LDOS of the clean anti-phase modulated system, thus enabling the appearance of the peaks

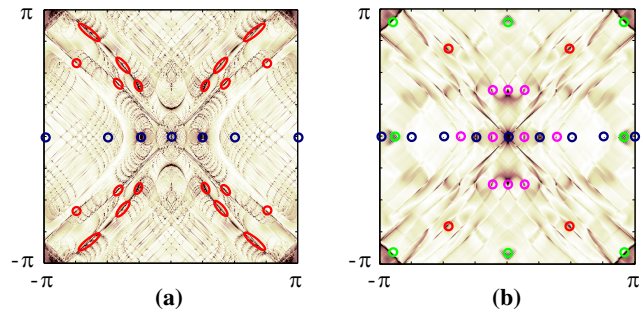


FIG. 12: FT-LDOS at  $\omega = 0$  of a model of LBCO with (a) anti-phase modulated DSC order and (b) coexisting anti-phase and homogeneous DSC orders. The amplitude of the modulated order is  $\Delta = 0.1t_1$  and that of the constant component is  $\Delta_0 = 0.01t_1$ . The results are for an impurity strength of  $V_0 = 150$  meV. Darker regions correspond to higher FT-LDOS and we have indicated high-intensity peaks by circles: Peaks associated with the modulation wave vector are encircled in blue. Peaks that correspond to scattering between the nodal points of the homogeneous DSC are marked in green. Peaks due to scattering between the additional nodal points which appear in the mixed phase are marked in pink. Other high-intensity peaks which are not simply related to scattering between nodal points are designated in red.

at  $(\pm\pi/4, 0)$ .] The positions in  $\mathbf{k}$ -space of many of the remaining peaks may be associated with wavevectors connecting high zero-energy LDOS regions of the clean system<sup>9,19</sup>. This is especially true for the case with additional homogeneous DSC where the zero-energy spectral weight appears at isolated nodal points. We were able to identify, as shown in Fig. 12, peaks which are associated with scattering between the nodal points of the homogeneous  $d$ -wave superconductors, as well as peaks which originate from scattering between the extra nodal points that are induced by the presence of the modulated DSC order, see Fig. 7. It is more difficult to trace the root of the peaks in the FT-LDOS of the pure modulated system, since it possesses an extended Fermi-surface.

### IV. CONCLUSIONS

We have identified several signatures which set apart the anti-phase modulated  $d$ -wave superconductor from other  $d$ -wave superconducting states. Most notably, we have shown that it supports a continuum of zero-energy excitations which form an extended Fermi-surface. The existence of such a Fermi-surface requires a pure  $\pi$ -phase shift of the superconducting order across the domains boundaries. The presence of a constant DSC order, no matter how weak, drastically modifies the manifold of zero-energy states and results in a Fermi surface which consists of isolated nodal points. Nevertheless, much of the low-energy spectral weight still concentrates along extended arcs in momentum space, and can be detected by ARPES measurements. ARPES can also be used to iden-

tify the additional nodal points which we predict exist under such circumstances, beside the conventional nodal points associated with a homogeneous  $d$ -wave order. The periodic modulation of the superconducting order can be traced using scanning tunneling spectroscopy, which can also detect the accompanying low-energy spectral weight, and the identifying features in the FT-LDOS of the anti-phase modulated superconductor.

### Acknowledgments

It is a pleasure to thank Erez Berg, Cheng-Chien Chen and Steve Kivelson for useful discussions and for sharing with us their results. This work was supported by the United States - Israel Binational Science Foundation (grant No. 2004162).

## APPENDIX A: THE HAMILTONIANS

### 1. Superconducting orders

The analysis of the various orders was carried out using mean-field Hamiltonians written in momentum space. The modulated superconducting orders are conveniently expressed in terms of the spinor  $\psi_{\mathbf{k}}^\dagger = (c_{\mathbf{k}\uparrow}^\dagger, c_{\mathbf{k}+\mathbf{q}\uparrow}^\dagger, \dots, c_{-\mathbf{k}\downarrow}, c_{-(\mathbf{k}+\mathbf{q})\downarrow}, \dots)$ , with  $\mathbf{q}$  the ordering wavevector, and  $\mathbf{k}$  varying over the reduced Brillouin zone (RBZ) associated with the order. In this basis the Hamiltonian

$$H = \sum_{\mathbf{k} \in \text{RBZ}} \psi_{\mathbf{k}}^\dagger \hat{H}_{\mathbf{k}} \psi_{\mathbf{k}}, \quad (\text{A1})$$

takes the form

$$\hat{H}_{\mathbf{k}} = \begin{pmatrix} \mathcal{A}_{\mathbf{k}} & \mathcal{C}_{\mathbf{k}} \\ \mathcal{C}_{\mathbf{k}}^\dagger & -\mathcal{A}_{\mathbf{k}} \end{pmatrix}, \quad (\text{A2})$$

where  $\mathcal{A}_{\mathbf{k}}$  is a diagonal matrix with entries  $\xi(\mathbf{k}), \xi(\mathbf{k} + \mathbf{q}), \dots$ , and where  $\mathcal{C}_{\mathbf{k}}$  contains the particle-particle couplings.

While the RBZ of the in-phase modulated superconductor is twice that of its anti-phase counterpart, we choose to describe both in the RBZ of the latter, i.e.,  $-q_x/2 < k_x < q_x/2$  and  $-\pi < k_y < \pi$ , where  $\mathbf{q} = (\pi/4, 0)$ . In this case  $\mathcal{C}_{\mathbf{k}}$  is an  $8 \times 8$  matrix,

$$\mathcal{C}_{\mathbf{k}} = \begin{pmatrix} f_0(\mathbf{k}) & f_1(\mathbf{k}) & \cdots & f_7(\mathbf{k}) \\ f_1^*(\mathbf{k}) & f_0(\mathbf{k} + \mathbf{q}) & \cdots & f_6(\mathbf{k} + \mathbf{q}) \\ \vdots & & \ddots & \\ f_7^*(\mathbf{k}) & & & f_0(\mathbf{k} + 7\mathbf{q}) \end{pmatrix}, \quad (\text{A3})$$

characterized by the functions  $f_n(\mathbf{k})$ .

The only non-vanishing contribution to the uniform superconducting order is

$$f_0(\mathbf{k}) = \frac{\Delta_0}{2} (\cos k_x - \cos k_y). \quad (\text{A4})$$

The real-space representation of the in-phase modulated superconducting Hamiltonian is given by Eq. (1). Since only integer  $x$  and  $y$  are of interest, when converting it to the momentum-space representation, we approximate the absolute value function by its first eight Fourier components, with the result

$$\begin{aligned} f_0(\mathbf{k}) &= \frac{\Delta}{8} [2\sqrt{2} \cos(q_x/2) \cos k_x - (1 + \sqrt{2}) \cos k_y], \\ f_2(\mathbf{k}) &= \frac{\Delta}{8} [\sqrt{2} \sin(q_x/2) (\cos k_x - \sin k_x) - \cos k_y], \\ f_4(\mathbf{k}) &= \frac{\Delta}{8} (-1 + \sqrt{2}) \cos k_y, \\ f_6(\mathbf{k}) &= f_2(\mathbf{k} + 6\mathbf{q}). \end{aligned} \quad (\text{A5})$$

In the presence of an anti-phase modulated superconducting order one obtains

$$\begin{aligned} f_1(\mathbf{k}) &= \frac{\Delta}{4} [\cos(k_x + q_x/2) - \cos k_y], \\ f_7(\mathbf{k}) &= \frac{\Delta}{4} [\cos(k_x - q_x/2) - \cos k_y]. \end{aligned} \quad (\text{A6})$$

### 2. Non-superconducting orders

For the Hamiltonians of the non-superconducting orders we use a similar representation to Eq. (A1), but with  $\psi_{\mathbf{k}}$  defined with respect to the wavevector  $\tilde{\mathbf{q}} = (\pi/4, \pi)$ . Here, we choose to let  $\mathbf{k}$  run over the RBZ of the modulated DDW and spin-stripe orders, despite it being half the size of the RBZ of the charge-stripe phase. The result is

$$\hat{H}_{\mathbf{k}} = \begin{pmatrix} \mathcal{A}_{\mathbf{k}} + \mathcal{B}_{\mathbf{k}} & 0 \\ 0 & -\mathcal{A}_{\mathbf{k}} - \eta \mathcal{B}_{\mathbf{k}} \end{pmatrix}, \quad (\text{A7})$$

where  $\eta = 1$  for the charge and DDW stripe phase, and  $\eta = -1$  in the case of spin-stripe order.  $\mathcal{B}_{\mathbf{k}}$  contains the particle-hole couplings

$$\mathcal{B}_{\mathbf{k}} = \begin{pmatrix} g_0(\mathbf{k}) & g_1(\mathbf{k}) & \cdots & g_7(\mathbf{k}) \\ g_1^*(\mathbf{k}) & g_0(\mathbf{k} + \tilde{\mathbf{q}}) & \cdots & g_6(\mathbf{k} + \tilde{\mathbf{q}}) \\ \vdots & & \ddots & \\ g_7^*(\mathbf{k}) & & & g_0(\mathbf{k} + 7\tilde{\mathbf{q}}) \end{pmatrix}, \quad (\text{A8})$$

The non-vanishing contributions in the charge-stripe phase are

$$\begin{aligned} g_0(\mathbf{k}) &= \frac{\Phi_{CDW}}{4} [1 + 2 \cos(\tilde{q}_x)], \\ g_2(\mathbf{k}) &= g_6(\mathbf{k}) = -\frac{\Phi_{CDW}}{4}, \\ g_4(\mathbf{k}) &= \frac{\Phi_{CDW}}{4} [1 - 2 \cos(\tilde{q}_x)], \end{aligned} \quad (\text{A9})$$

where the absolute value function was again approximated using the low harmonics. The  $g_0(\mathbf{k})$  term renormalizes the chemical potential. The latter was chosen to maintain the desired hole doping.

The spin-stripe phase is characterized by the following terms

$$g_3(\mathbf{k}) = -g_5(\mathbf{k}) = i \frac{\Phi_{AF}}{4}. \quad (\text{A10})$$

We considered an anti-phase, period-8, modulated version of the d-density wave, (see Fig. 3). The corresponding real-space order parameter is

$$\begin{aligned} \langle c_{\mathbf{r},\sigma}^\dagger c_{\mathbf{r}',\sigma} \rangle &= i \frac{\Phi_{DDW}}{2} (-1)^{x+y} \\ &\times \left\{ 2\delta_{\mathbf{r}',\mathbf{r}+\hat{x}} \Theta_{\tilde{q}_x}(x) + 2\delta_{\mathbf{r}',\mathbf{r}-\hat{x}} \Theta_{\tilde{q}_x}(x-1) \right. \\ &\left. - (\delta_{\mathbf{r}',\mathbf{r}+\hat{y}} + \delta_{\mathbf{r}',\mathbf{r}-\hat{y}}) [\Theta_{\tilde{q}_x}(x) + \Theta_{\tilde{q}_x}(x-1)] \right\}, \end{aligned} \quad (\text{A11})$$

where  $\Theta_{q_x}(x)$  is a periodic variation of the usual heavy-side function, *i.e.*

$$\Theta_{q_x}(x) = \begin{cases} 1 & 2\pi n/q_x < x < (2n+1)\pi/q_x \\ -1 & (2n-1)\pi/q_x < x < 2\pi n/q_x \\ 0 & x = n\pi/q_x \end{cases} \quad (\text{A12})$$

for all integers  $n$ . The corresponding functions entering the momentum-space Hamiltonian are given by

$$\begin{aligned} g_1(\mathbf{k}) &= h(\mathbf{k}, 5\tilde{q}_x/2), \\ g_3(\mathbf{k}) &= h(\mathbf{k}, 7\tilde{q}_x/2), \\ g_5(\mathbf{k}) &= h(\mathbf{k}, -7\tilde{q}_x/2), \\ g_7(\mathbf{k}) &= h(\mathbf{k}, -5\tilde{q}_x/2), \end{aligned} \quad (\text{A13})$$

where

$$\begin{aligned} h(\mathbf{k}, q_x) &= \Phi_{DDW} e^{iq_x} \sin(4q_x) [1 + 2\cos(2q_x)] \\ &\times [\cos(k_x + q_x) - \cos(k_y) \cos(q_x)]. \end{aligned} \quad (\text{A14})$$

### 3. Combining the orders

When superconducting and non-superconducting orders coexist we need to expand our basis to include them both. We use

$$\begin{aligned} \psi_{\mathbf{k}}^\dagger &= (c_{\mathbf{k}\uparrow}^\dagger, c_{\mathbf{k}+(q_x,0)\uparrow}^\dagger, \dots, c_{\mathbf{k}+(7q_x,0)\uparrow}^\dagger, c_{\mathbf{k}+(q_x,\pi)\uparrow}^\dagger, \dots, \\ &c_{\mathbf{k}+(7q_x,\pi)\uparrow}^\dagger, c_{-\mathbf{k}\downarrow}, c_{-\mathbf{k}+(q_x,0)\downarrow}, \dots, c_{-\mathbf{k}+(7q_x,\pi)\downarrow}). \end{aligned} \quad (\text{A15})$$

The combined Hamiltonian is 32-dimensional and is defined in the momentum-space region  $-q_x/2 < k_x < q_x/2$ , and  $-\pi/2 < k_y < \pi/2$ . The terms in this Hamiltonian are determined by adding the corresponding terms, connecting the same momenta, in Hamiltonians (A2) and (A7).

### APPENDIX B: CALCULATING THE FT-LDOS

The clean system can be described in terms of the spinor  $\psi_{\mathbf{k}}^\dagger$  defined in appendix A. In this basis the Hamiltonian is  $H = \sum_{\mathbf{k} \in RBZ} \psi_{\mathbf{k}}^\dagger \hat{H}_{\mathbf{k}} \psi_{\mathbf{k}}$ , where  $\hat{H}_{\mathbf{k}}$  is a model dependent matrix. The Green's function of the clean system,  $\hat{G}^0(\mathbf{k}, \omega)$ , is obtained by analytically continuing  $\hat{G}^0(\mathbf{k}, i\omega_n) = [i\omega_n I - \hat{H}_{\mathbf{k}}]^{-1}$ , via  $i\omega_n \rightarrow \omega + i\delta$ , where  $I$  is the identity matrix. In the numerical calculations we have used an energy broadening of  $\delta = 0.5$  meV.

The impurity scattering problem can be simplified by working in the Nambu basis in real space,  $(c_{\mathbf{r}\uparrow}^\dagger, c_{\mathbf{r}\downarrow})$ . The transformation of the Green's function between the two representations is given by

$$\begin{aligned} \hat{G}^0(\mathbf{r}, \mathbf{r}'; \omega) &= \frac{1}{(2\pi)^2} \sum_{\mathbf{k} \in RBZ} e^{i\mathbf{k}(\mathbf{r}-\mathbf{r}')} \\ &\times \begin{pmatrix} \phi^\dagger(\mathbf{r}) G_{11}^0(\mathbf{k}, \omega) \phi(\mathbf{r}') & \phi^\dagger(\mathbf{r}) G_{12}^0(\mathbf{k}, \omega) \phi(\mathbf{r}') \\ \phi^\dagger(\mathbf{r}) G_{21}^0(\mathbf{k}, \omega) \phi(\mathbf{r}') & \phi^\dagger(\mathbf{r}) G_{22}^0(\mathbf{k}, \omega) \phi(\mathbf{r}') \end{pmatrix}, \end{aligned} \quad (\text{B1})$$

where  $\phi^\dagger(\mathbf{r}) = (1, e^{i\mathbf{q}\mathbf{r}}, e^{2i\mathbf{q}\mathbf{r}}, \dots)$ , and  $G_{ij}^0$ ,  $i, j = 1, 2$ , are the four blocks comprising  $\hat{G}^0(k, \omega)$ .

We have included the impurity scattering in the T-matrix approximation<sup>25</sup>, which implies the following equation for the electronic Green's function

$$\begin{aligned} \hat{G}(\mathbf{r}, \mathbf{r}'; \omega_n) &= \hat{G}^0(\mathbf{r}, \mathbf{r}'; \omega) \\ &+ \int d\mathbf{r}_1 d\mathbf{r}_2 \hat{G}^0(\mathbf{r}, \mathbf{r}_1; \omega) \hat{T}(\mathbf{r}_1, \mathbf{r}_2; \omega) \hat{G}^0(\mathbf{r}_2, \mathbf{r}'; \omega). \end{aligned} \quad (\text{B2})$$

For simplicity we have assumed scattering off a non-magnetic  $\delta$ -function impurity centered at the origin. Under such conditions the T-matrix is given by  $\hat{T}(\mathbf{r}, \mathbf{r}'; \omega) = [V_0^{-1} \tau_3 - \hat{G}^0(0; \omega)]^{-1} \delta(\mathbf{r}) \delta(\mathbf{r}')$ , where  $V_0$  is the impurity strength and  $\tau$  are the Pauli matrices. The local density of states at a point  $\mathbf{r}$  in the sample is then given by  $\rho(\mathbf{r}, \omega) = -\frac{1}{\pi} \text{Im}[G_{11}(\mathbf{r}, \mathbf{r}; \omega) + G_{22}(\mathbf{r}, \mathbf{r}; -\omega)]$ , from which the FT-LDOS is readily obtained.

<sup>1</sup> For a review of some of the experimental evidence for the existence of meso-structure in the cuprates and its possible relation to the mechanism of high temperature superconductivity see E. W. Carlson, V. J. Emery, S. A. Kivelson, and D. Orgad, in "The Physics of Superconductors:

*Superconductivity in Nanostructures, High-T<sub>c</sub> and Novel Superconductors, Organic Superconductors*", Vol 2, p. 275, edited by K. H. Bennemann and J. B. Ketterson (Springer-Verlag 2004).

<sup>2</sup> S. H. Pan, J. P. O'Neal, R. L. Badzey, C. Chamon,

- H. Ding, J. R. Engelbrecht, Z. Wang, H. Eisaki, S. Uchida, A. K. Gupta, K.-W. Ng, E. W. Hudson, K. M. Lang, and J. C. Davis, *Nature (London)* **413**, 282 (2001).
- <sup>3</sup> K. M. Lang, V. Madhavan, J. E. Hoffman, E. W. Hudson, H. Eisaki, S. Uchida, and J. C. Davis, *Nature (London)* **415**, 412 (2002).
  - <sup>4</sup> T. Kato, S. Okitsu, and H. Sakata, *Phys. Rev. B* **72**, 144518 (2005).
  - <sup>5</sup> K. McElroy, J. Lee, J. A. Slezak, D. H. Lee, H. Eisaki, S. Uchida, and J. C. Davis, *Science* **309**, 1048 (2005).
  - <sup>6</sup> R. Jamei, J. Robertson, E.-A. Kim, A. Fang, A. Kapitulnik, and S. A. Kivelson, *Phys. Rev. B* **74**, 174521 (2006).
  - <sup>7</sup> A. C. Fang, L. Capriotti, D. J. Scalapino, S. A. Kivelson, N. Kaneko, M. Greven, and A. Kapitulnik, *Phys. Rev. Lett.* **96**, 017007 (2006).
  - <sup>8</sup> J. E. Hoffman, E. W. Hudson, K. M. Lang, V. Madhavan, H. Eisaki, S. Uchida, and J. C. Davis, *Science* **295**, 466 (2002).
  - <sup>9</sup> J. E. Hoffman, K. McElroy, D.-H. Lee, K. M. Lang, H. Eisaki, S. Uchida, and J. C. Davis, *Science* **297**, 1148 (2002).
  - <sup>10</sup> K. McElroy, R. W. Simmonds, J. E. Hoffman, D.-H. Lee, J. Orenstein, H. Eisaki, U. Uchida, and J. C. Davis, *Nature (London)* **422**, 592 (2003).
  - <sup>11</sup> C. Howald, H. Eisaki, N. Kaneko, M. Greven, and A. Kapitulnik, *Phys. Rev. B* **67**, 014533 (2003).
  - <sup>12</sup> T. Hanaguri, C. Lupien, Y. Kohsaka, D.-H. Lee, M. Azuma, M. Takano, H. Takagi, and J. C. Davis, *Nature (London)* **430**, 1001 (2004).
  - <sup>13</sup> A. Fang, C. Howald, N. Kaneko, M. Greven and, A. Kapitulnik, *Phys. Rev. B* **70**, 214514 (2004).
  - <sup>14</sup> M. Vershinin, S. Misra, S. Ono, Y. Abe, Y. Ando and A. Yazdani, *Science* **303**, 1995 (2004).
  - <sup>15</sup> K. McElroy, D.-H. Lee, J. E. Hoffman, K. M. Lang, J. Lee, E. W. Hudson, H. Eisaki, S. Uchida, and J. C. Davis, *Phys. Rev. Lett.* **94**, 197005 (2005).
  - <sup>16</sup> A. Hashimoto, N. Momono, M. Oda, and M. Ido, *Phys. Rev. B* **74**, 064508 (2006).
  - <sup>17</sup> Y. Kohsaka, C. Taylor, K. Fujita, A. Schmidt, C. Lupien, T. Hanaguri, M. Azuma, M. Takano, H. Eisaki, H. Takagi, S. Uchida, and J. C. Davis, *Science* **315**, 1380 (2007).
  - <sup>18</sup> A. Melikyan and Z. Tešanović, *Phys. Rev. B* **71**, 214511 (2005).
  - <sup>19</sup> Q.-H. Wang and D.-H. Lee, *Phys. Rev. B* **67**, 020511(R) 2003.
  - <sup>20</sup> D. Podolsky, E. Demler, K. Damle, and B. I. Halperin, *Phys. Rev. B* **67**, 094514 (2003).
  - <sup>21</sup> E. Berg, E. Fradkin, E.-A. Kim, S. A. Kivelson, V. Oganesyan, J. M. Tranquada, and S. C. Zhang, *Phys. Rev. Lett.* **99**, 127003 (2007).
  - <sup>22</sup> A. Himeda, T. Kato, and M. Ogata, *Phys. Rev. Lett.* **88**, 117001 (2002).
  - <sup>23</sup> Q. Li, M. Hücker, G. D. Gu, A. M. Tsvelik, and J. M. Tranquada, *Phys. Rev. Lett.* **99**, 067001 (2007).
  - <sup>24</sup> M. Raczkowski, M. Capello, D. Poilblanc, R. Frésard, and A. M. Oleś, *Phys. Rev. B* **76**, 140505 (2007).
  - <sup>25</sup> For a review see A. V. Balatsky, I. Vekhter, and J.-X. Zhu, *Rev. Mod. Phys.* **78**, 373 (2006).
  - <sup>26</sup> T. Pereg-Barnea and M. Franz, *Phys. Rev. B* **68**, 180506(R) (2003).
  - <sup>27</sup> C.-T. Chen and N.-C. Yeh, *Phys. Rev. B* **68**, 220505(R) (2003).
  - <sup>28</sup> H.-Y. Chen and C. S. Ting, *Phys. Rev. B* **68**, 212502 (2003).
  - <sup>29</sup> C. Bena, S. Chakravarty, J. Hu, and C. Nayak, *Phys. Rev. B* **69**, 134517 (2004).
  - <sup>30</sup> S. Misra, M. Vershinin, P. Phillips, and A. Yazdani, *Phys. Rev. B* **70**, 220503(R) (2004).
  - <sup>31</sup> D. Zhang and C. S. Ting, *Phys. Rev. B* **69**, 012501 (2004).
  - <sup>32</sup> W. A. Atkinson, *Phys. Rev. B* **71**, 024516 (2005).
  - <sup>33</sup> M. Cheng and W. P. Su, *Phys. Rev. B* **72**, 094512 (2005).
  - <sup>34</sup> L. Dell'Anna, J. Lorenzana, M. Capone, C. Castellani, and M. Grilli, *Phys. Rev. B* **71**, 064518 (2005).
  - <sup>35</sup> A. Gohsal, A. Kopp, and S. Chakravarty, *Phys. Rev. B* **72**, 220502(R) (2005).
  - <sup>36</sup> H.-Y. Chen and C. S. Ting, *Phys. Rev. B* **71**, 220510(R) (2005).
  - <sup>37</sup> T. S. Nunner, W. Chen, B. M. Andersen, A. Melikyan, and P. J. Hirschfeld, *Phys. Rev. B* **73**, 104511 (2006).
  - <sup>38</sup> M. R. Norman, M. Randeria, H. Ding, and J. C. Campuzano, *Phys. Rev. B* **52**, 615 (1995).
  - <sup>39</sup> We adopt the value of  $t_1$  from the band-structure of  $\text{La}_2\text{CuO}_4$  as appears in E. Pavarini, I. Dasgupta, T. Saha-Dasgupta, O. Jepsen, and O. K. Andersen, *Phys. Rev. Lett.* **87**, 047003 (2001). The values of  $t_2$  was averaged over several band-structure calculations for  $\text{La}_{2-x}\text{Sr}_x\text{CuO}_4$ .
  - <sup>40</sup> S. Chakravarty, R. B. Laughlin, D. K. Morr, and C. Nayak, *Phys. Rev. B* **63**, 094503 (2001).
  - <sup>41</sup> Y. Tanaka and S. Kashiwaya, *Phys. Rev. B* **53**, 9371 (1996).
  - <sup>42</sup> N. Doiron-Leyraud, C. Proust, D. LeBoeuf, J. Levallois, J.-B. Bonnemaison, R. Liang, D. A. Bonn, W. N. Hardy, and L. Taillefer, *Nature* **447**, 565 (2007).
  - <sup>43</sup> C. Jaudet, D. Vignolles, A. Audouard, J. Levallois, D. LeBoeuf, N. Doiron-Leyraud, B. Vignolle, M. Nardone, A. Zitouni, R. Liang, D. A. Bonn, W. N. Hardy, L. Taillefer, and C. Proust, arxiv/0711.3559.
  - <sup>44</sup> M. Granath, arxiv/0711.2009 (unpublished).
  - <sup>45</sup> A. J. Millis and M. R. Norman, *Phys. Rev. B* **76**, 220503(R) (2007).